DISEASE-SPECIFIC

PROBABILISTIC BRAIN ATLASES

[1]Paul Thompson PhD, [1,2]Michael S. Mega MD PhD, [1]Arthur W. Toga PhD

[1]Laboratory of Neuro Imaging, Dept. of Neurology, Division of Brain Mapping,
UCLA School of Medicine, Los Angeles, CA
[2]Alzheimer's Disease Center, UCLA School of Medicine, Los Angeles, CA

IEEE Workshop on
Mathematical Methods in Biomedical Image Analysis
Hilton Head Island, South Carolina
June 11-12, 2000

Theme: Computational Anatomical Atlases
Length: 8 pages, including figures and references, CVPR Submission Format

Please address correspondence to:
Dr. Paul Thompson
(Rm. 4238, Reed Neurological Research Center)
Laboratory of Neuro Imaging, Dept. of Neurology, UCLA School of Medicine
710 Westwood Plaza, Los Angeles, CA 90095-1769
Phone: (310) 206-2101 **Fax:** (310) 206-5518 **E-mail:** thompson@loni.ucla.edu

Disease-Specific Probabilistic Brain Atlases

[1]Paul Thompson PhD, [1,2]Michael S. Mega MD PhD, [1]Arthur W. Toga PhD

[1]Laboratory of Neuro Imaging, Dept. of Neurology, Division of Brain Mapping,
UCLA School of Medicine, Los Angeles, CA
[2]Alzheimer's Disease Center, UCLA School of Medicine, Los Angeles, CA

Abstract

Atlases of the human brain, in health and disease, provide a comprehensive framework for understanding brain structure and function. The complexity and variability of brain structure, especially in the gyral patterns of the human cortex, present challenges in creating standardized brain atlases that reflect the anatomy of a population. This paper introduces the concept of a population-based, disease-specific brain atlas that can reflect the unique anatomy and physiology of a particular clinical subpopulation. Based on well-characterized patient groups, disease-specific atlases contain thousands of structure models, composite maps, average templates, and visualizations of structural variability, asymmetry and group-specific differences. They correlate the structural, metabolic, molecular and histologic hallmarks of the disease. Rather than simply fusing information from multiple subjects and sources, new mathematical strategies are introduced to resolve group-specific features not apparent in individual scans. High-dimensional elastic mappings, based on covariant partial differential equations, are developed to encode patterns of cortical variation. In the resulting brain atlas, disease-specific features and regional asymmetries emerge that are not apparent in individual anatomies. The resulting probabilistic atlas can identify patterns of altered structure and function, and can guide algorithms for knowledge-based image analysis, automated image labeling, tissue classification, data mining and functional image analysis.

1 Introduction

Advanced brain imaging technologies now provide a means to investigate disease and therapeutic response in their full spatial and temporal complexity. Imaging studies of clinical populations continue to uncover new patterns of altered structure and function, and novel algorithms are being applied to relate these patterns to cognitive and genetic parameters. As imaging studies expand into ever-larger patient populations, population-based brain atlases will offer a powerful framework to synthesize the results of disparate imaging studies. These atlases require novel analytical tools to fuse data across subjects, modalities, and time, enabling detection of group-specific features not apparent in individual patients' scans. Once built, these atlases can be stratified into subpopulations to reflect a particular clinical group. The disease-specific features they resolve can then be linked with demographic factors such as age, gender, handedness, as well as specific clinical or genetic parameters [1].

Imaging algorithms are rapidly increasing the flexibility of digital brain templates. *Deformable brain atlases* [2] are adaptable brain templates that can be individualized to reflect the anatomy of new subjects. *Probabilistic atlases* [1,3,4] store detailed information on structural and functional variability. These atlases can be used to detect altered structure and function in an individual or group, and the information they store on anatomic variation can guide automated image labeling, data mining, and functional image analysis.

Despite the interest in relating population-based functional, anatomic, histologic and molecular data in diseases such as Alzheimer's disease and schizophrenia, current population-based brain templates poorly represent the anatomy of these clinical populations. Because the anatomy is altered in these diseases (reviewed in [5,6]), it is desirable to register and correlate data in an atlas coordinate system that reflects the morphology of the clinical population so that least distortion is applied. The result is an image analysis framework that relates the structural, functional, metabolic and pathologic characteristics of the disease in a 3D reference coordinate system. The atlas also supports the exploration of linkages between these imaging data and therapeutic response, as well as dynamic data on local anatomic change [6,7] and cognitive and behavioral parameters ([8]; Fig. 1).

Central to the construction of a disease-specific atlas is the creation of averages, templates and models to describe how the brain and its component parts are organized, and how they are altered in disease. Statistical models are created to reveal how major anatomic systems are affected, how the pathology progresses, and how these changes relate to
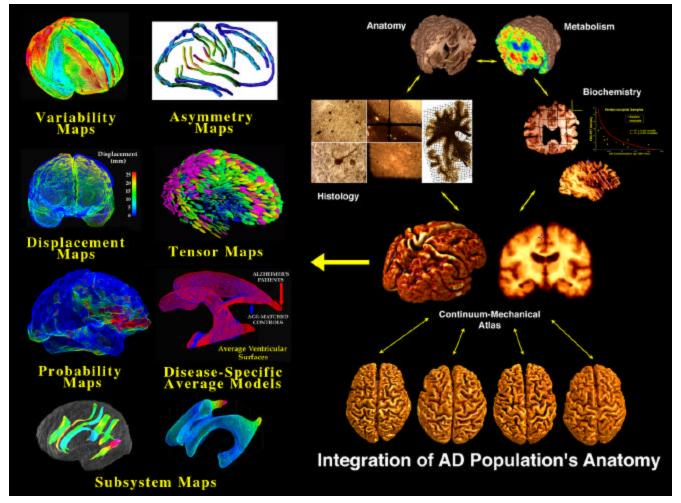
Figure 1. *Elements of a Disease-Specific Atlas.* This schematic shows the types of maps and models contained in a disease-specific brain atlas. This atlas represents an Alzheimer's Disease population. To construct the atlas, databases of structural imaging data are used to develop detailed models of cortical structure and anatomic subsystems. These models are statistically combined to create group average models that can be compared with averages from elderly normal subjects matched for age, gender, handedness and educational level. Patterns of 3D structural variability, asymmetry, and disease-specific differences are also computed from the anatomic data. A well-resolved average image template for the patient population (*Continuum-Mechanical Atlas*, *center right*) is created by (1) using high-dimensional surface-based 3D warping to reconfigure each subject's anatomy to match an average set of 84 surfaces defined for the group, and then (2) voxel-wise averaging of normalized image intensities across the group. Surface-based warping ensures that boundaries in the mean image template are consistent with the averaged anatomic surface data contained in the atlas. Given this mean image template, intensity-based image registration approaches can then also be used to automatically align MRI, PET and SPECT (magnetic resonance imaging and positron emission/single photon emission computed tomography) data with the atlas. The resulting coordinate framework links *in vivo* metabolic and functional data with fine-scale anatomy and biochemistry (*top right*). In recent studies [9,10], histologic and biochemical maps of *post mortem* markers, including beta-amyloid protein distribution and neurofibrillary tangle (NFT) staining density, were correlated with *in vivo* metabolism. Using the algorithm of [11] (*warped image*), distorted tissue sections were elastically warped back to their configuration in the cryosection blockface (*top row*). A further 3D registration projected the data into pre-mortem MRI and co-registered PET data (*top right*).

------

demographic or genetic factors. To create templates that reflect the morphology of a diseased group, specialized strategies are required for population-based averaging of anatomy [2,12-14]. In one approach [5], sets of high-dimensional elastic mappings, based on the principles of continuum mechanics, reconfigure the anatomy of a large number of subjects in an anatomic image database. These 3D deformation fields are used to create an anatomical image template with highly-resolved structures in their mean spatial location. The mappings also generate a detailed local encoding of anatomic variability, with up to a billion parameters [2,15]. The resulting variability parameters are stored as a tensor field providing automated identification of anatomical structures in new patients' scans, and descriptions of disease-specific characteristics [4].

In this paper, we illustrate our atlasing approach by using high-dimensional transformations to create a disease-specific image template and a variety of average anatomical maps for an Alzheimer's disease population. The resulting mean anatomic templates reveal patterns of cortical variation, asymmetries and disease-related differences that are not apparent in individual anatomies, and illustrate the potential of the atlasing approach.

2 Methods

Imaging. High-resolution 3D ($256^2 \times 124$) T_1-weighted fast SPGR (spoiled GRASS) MRI volumes were acquired from 26 subjects diagnosed with mild to moderate Alzheimer's Disease (AD; NINCDS-ADRDA criteria) and 20 elderly control subjects. All subjects were matched for age (75.8 ± 1.7 yrs.), educational level (15.2 ± 0.4 yrs.), gender, and handedness (all 46 right-handed). All patients were matched for disease severity (mean Mini-Mental State Exam score: 20.0 ± 0.8, comparable with other studies of mild AD). Scan acquisition parameters were TR/TE 14.3/3.2 msec, flip angle 35°, NEX=1, FOV 25cm, with contiguous 1.5-mm thick slices (no interslice gap) covering the entire brain. Image data were *initially* transformed into a Talairach-based coordinate system [16] which (1) places the anterior commissure (AC) at the origin; (2) vertically orients the midsagittal plane; and (3) horizontally orients the AC-PC line. Aligned MR volumes were corrected for non-uniformity of MR signal intensity [17], and high-resolution surface models of the cerebral cortex were extracted, as described previously [3,18].

Cortical Patterns. 36 major external fissures and sulci in the brain were manually outlined on highly magnified surface-rendered images of each cortical surface. Detailed anatomic criteria were applied as set out in [3] and the Ono sulcal atlas [19] to define sulci whose topological consistency has been demonstrated across normal populations. In both brain hemispheres, 3D curves were drawn to represent superior and inferior frontal, central, postcentral, intraparietal, superior and inferior temporal, collateral, olfactory and occipito-temporal sulci, as well as the Sylvian fissures. Additional 3D curves were drawn in each hemisphere to represent gyral limits at the interhemispheric margin [3]. Stereotaxic locations of contour points derived from the data volumes were redigitized to produce 36 uniformly parameterized cortical contours per brain, representing the primary gyral pattern of each subject [3].

Gyral Pattern Matching. Due to variations in gyral patterning, cortical variability is severely underestimated unless elements of the gyral pattern are matched from one subject to another (*cf.* [3,4,11,20-24]). This matching is also required for cortical averaging; otherwise, corresponding

gyral features will not be averaged together. To find good matches among cortical regions we perform the matching process in the cortical surface's parametric space, which permits more tractable mathematics (Fig. 2; [3,4,24]). This vector flow field in the parametric space indirectly specifies a correspondence field in 3D, which drives one cortical surface into the shape of another. This mapping not only matches overall cortical geometry, but matches the entire network of the 36 landmark curves with their counterparts in the target brain, and thus is a valid encoding of cortical variation.

Spherical, Planar Maps of Cortex. Several simpler maps of the cortex are made to help calculate the transformation. Because each subject's cortical model is created by deforming a spherical mesh [11,18,22], any point on the cortex maps to exactly one point on the sphere, and a *spherical map* of the cortex can be made which indexes sulcal landmarks in the normally folded brain surface. These spherical locations, indexed by two parameters, can also be mapped to a plane (Fig. 2; [3,15]). A flow field is then calculated that elastically warps one flat map onto the other (Fig. 2; or equivalently, one spherical map to the other). On the sphere, the parameter shift function $\mathbf{u(r)}:\Omega \rightarrow \Omega$, is given by the solution $F_{pq}:\mathbf{r} \rightarrow \mathbf{r}-\mathbf{u(r)}$ to a curve-driven warp in the spherical parametric space $\Omega=[0,2\pi]\times[0,\pi]$ of the cortex [3,15]. For points $\mathbf{r}=(r,s)$ in the parameter space, a system of simultaneous partial differential equations can be written for the flow field $\mathbf{u(r)}$:

$$L^{\ddagger}(\mathbf{u(r)}) + \mathbf{F(r-u(r))} = \mathbf{0}, \ \forall \mathbf{r} \in \Omega, \text{ with } \mathbf{u(r)} = \mathbf{u_0(r)},$$
$$\forall \mathbf{r} \in M_0 \cup M_1. \qquad (1)$$

Here M_0, M_1 are sets of points and (sulcal or gyral) curves where displacement vectors $\mathbf{u(r)}=\mathbf{u_0(r)}$ matching corresponding anatomy across subjects are known. The flow behavior is modeled using equations derived from continuum mechanics, and these equations are governed by the Cauchy-Navier differential operator $L = \mu\nabla^2+(\lambda+\mu)\nabla(\nabla^T\bullet)$ with body force $\mathbf{F}$ (Thompson et al., 1996, 1998, 1999; Grenander and Miller, 1998). The only difference is that $L^{\ddagger}$ is the *covariant* form of the differential operator L (for reasons explained in *Footnote 1*).

Footnote 1: Covariant Field Equations. Since the cortex is not a *developable* surface [22], it cannot be given a parameterization whose metric tensor is uniform. As in fluid dynamics or general relativity applications, the intrinsic curvature of the solution domain can be taken into account when computing flow vector fields in the cortical parameter space, and mapping one mesh surface onto another. In the *covariant tensor* approach [4], correction terms (Christoffel symbols, $\mathbf{\Gamma}^i_{jk}$) make the necessary adjustments for
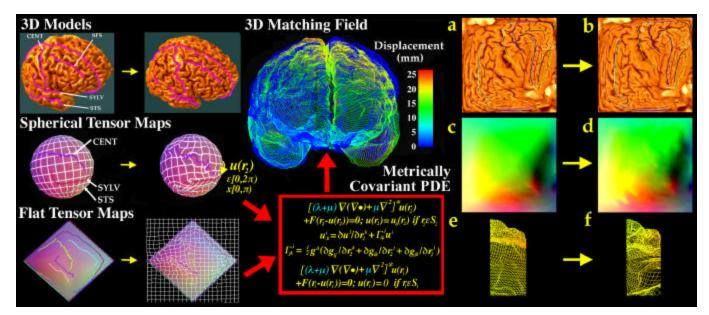
Figure 2. *Computing Differences in Cortical Patterns.* Cortical anatomy can be compared, for any pair of subjects (*3D Models; top left*), by computing the 3D deformation field that reconfigures one subject's cortex onto another (*3D Matching Field, middle panel*). In this mapping, gyral patterns must also be constrained to match their counterparts in the target brain. To do this, deformable surface extraction of the cortex provides a continuous inverse mapping from each subject's cortex to a sphere or plane. A vector field **u(r)** in the parameter space then drives the network elements into register on the sphere (*see spherical flow*). The full mapping (*top middle*) can be recovered in 3D space as a displacement vector field that drives cortical points and regions in one brain into precise structural registration with their counterparts in the other brain. *Tensor Maps (middle and lower left):* Although these simple 2-parameter surfaces can serve as proxies for the cortex, different amounts of local dilation and contraction (encoded in the metric tensor of the mapping, $g_{jk}(\mathbf{r})$) are required to transform the cortex into a simpler 2-parameter surface. These variations complicate the direct application of 2D regularization equations for matching their features. Using a covariant tensor approach (*red box*) the regularization operator L is replaced by its covariant form L^*, in which correction terms (Christoffel symbols, $\mathbf{\Gamma}^i_{jk}$) compensate for fluctuations in the metric tensor of the flattening procedure. This (1) makes the matching field invariant to the underlying parameterization (spherical or planar), and (2) eliminates confounding effects of metric distortions that occur during the flattening procedure. *Right panels, (a)-(f):* Gyral patterns can also be matched across a *group* of subjects to create *average* cortical surfaces. (a) shows a cortical flat map for the left hemisphere of one subject, with the average cortical pattern for the group overlaid (*colored lines*). (b) shows the result of warping the individual's sulcal pattern into the average configuration for the group, using the covariant field equations. The 3D cortical regions that map to these average locations are then recovered in each individual subject, as follows. A color code ((c), Thompson and Toga, 1997) representing 3D cortical point locations (e) in this subject is convected along with the flow that drives the sulcal pattern into the average configuration for the group (d). Once this is done in all subjects, points on each individual's cortex are recovered (f) that have the same relative location to the primary folding pattern in all subjects. Averaging of these corresponding points results in a crisp average cortex (Fig. 3(c), *top panel*). The transformation fields that map individuals onto the group average are stored and used to measure regional variability (Fig. 4).

----

fluctuations in the metric tensor of the mapping procedure. In the partial differential equations (1), we replace L by the covariant differential operator $L^{\ddagger}$. In $L^{\ddagger}$, all L's partial derivatives are replaced with covariant derivatives. These covariant derivatives are defined with respect to the metric tensor of the surface domain where calculations are performed. The covariant derivative of a (contravariant) vector field, $u^i(\mathbf{x})$, is defined as $u^i_{,k} = \partial u^i/\partial x^k + \mathbf{\Gamma}^i_{ik} u^i$ where the *Christoffel symbols of the second kind* [25], $\mathbf{\Gamma}^i_{ik}$, are computed from derivatives of the metric tensor components $g_{jk}(\mathbf{x})$:

$$\mathbf{\Gamma}^i_{jk} = (1/2)\, g^{il}\, (\partial g_{lj}/\partial x^k + \partial g_{lk}/\partial x^j - \partial g_{jk}/\partial x^i). \qquad (2)$$

These correction terms are then used in the solution of the Dirichlet problem [26] to match one cortex with another. Note that a parameterization-invariant variational formulation could also be used to minimize metric distortion when mapping one surface to another. If P and Q are cortical surfaces with metric tensors $g_{jk}(u^i)$ and $h_{jk}(\xi^\alpha)$ in local coordinates u^i and ξ^α ($i, \alpha = 1,2$), the *Dirichlet energy* of the mapping $\xi(u)$ is defined as: $E(\xi) = \int_P e(\xi)(u)\, dP$, where $e(\xi)(u) = g^{ij}(u)\, \partial\xi^\alpha(u)/\partial u^i\, \partial\xi^\beta(u)/\partial u^j\, h_{\alpha\beta}(\xi(u))$ and $dP = (\sqrt{\det[g_{ij}]})du^1 du^2$. The Euler equations, whose solution $\xi^\alpha(u)$ minimizes the mapping energy, are:

$$0 = L(\xi^i) = \Sigma_{m=1\,\text{to}\,2}\, \partial/\partial u^m\, [(\sqrt{\det[g^{ru}]})\, \Sigma_{l=1\,\text{to}\,2}\, g^{ml}_{ur}\, \partial\xi^i/\partial u^l]$$
$$(i=1,2),$$

[27]. The resulting (harmonic) map (1) minimizes the change in metric from one surface to the other, and (2) is again independent of the parameterizations (spherical or planar) used for each surface.

Creating an Average Cortical Surface. The warping field deforming one cortex into gyral correspondence with another can also be used to create an *average* model of the cortex. To do this, all 36 gyral curves for all subjects are first transferred to the spherical parameter space. Next, each curve is uniformly re-parameterized to produce a regular curve of 100 points on the sphere whose corresponding 3D locations are uniformly spaced. A set of 36 average gyral curves for the group is created by vector averaging all point locations on each curve. This *average curve template* (*curves* in Fig. 2(b)) serves as the target for alignment of individual cortical patterns (*cf.* [24]). Each individual cortical pattern is transformed into the average curve configuration using a flow field within the parameter space (Fig. 2(a),(b)). By carrying a color code (that indexes 3D locations) along with the vector flow that aligns each individual with the average folding pattern, information can be recovered at a particular location in the average folding pattern (Fig. 2(d)) specifying the 3D cortical points mapping each subject to the average. This produces a new coordinate grid on a given subject's cortex (Fig. 2(f)) in which particular grid-points appear in the same location across subjects relative to the mean gyral pattern. By averaging these 3D positions across subjects, an average 3D cortical model can be constructed for the group (Fig. 3, *right panels)*. The resulting mapping is guaranteed to average together all points falling on the same cortical locations across the set of brains, and ensures that corresponding features are averaged together (Fig. 3(c)).

Average Image Template Construction. High-dimensional cortical transformations also permit the construction of a disease-specific image template with the average image intensity and geometry for the AD population (Fig. 3(c)). By averaging geometric and intensity features separately [2,29], the resulting brain template has well-resolved cortical features in their mean anatomic location. To produce an average template for the group, 9 brains were selected for which a set of 84 anatomic surface models had been created [14]. An initial image template for the group was constructed by (1) using automated linear transformations [30] to align the MRI data with a randomly selected image, (2) intensity-averaging the aligned scans, and then (3) recursively re-registering the scans to the resulting average affine image. The resulting average image was adjusted to to align the MRI data with a randomly selected image, (2) intensity-averaging the aligned scans, and then (3) recursively re-registering the scans to the resulting average affine image. The resulting average image was adjusted to have the mean affine shape for the group [31]. Images and surface models were then linearly aligned to this template, and an average surface set was created for the group [14]. Displacement maps (Fig. 3(e)) driving the surface anatomy of each subject into correspondence with the average surface set were then extended to the full volume with a 3D warping
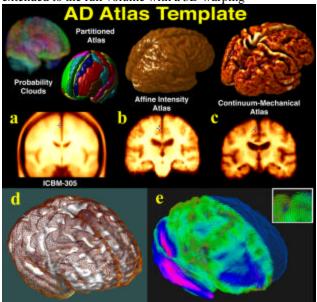

Figure 3. *Average Brain Templates*. (a) In a widely-used average brain image template (ICBM305) based on voxel-wise intensity averaging of 305 young normal subjects' scans [28], anatomical features are not well-resolved at the cortex. Cortical variability is represented using probability clouds (*top left*) that describe the frequency of incidence for each gyrus at each stereotaxic voxel, after linear registration and voxel-by-voxel comparison. In an affine brain template (b), similarly constructed from Alzheimer's disease patients' scans, the cortical average is also poorly resolved. By contrast, anatomical features are highly resolved, even at the cortex, in the *Continuum-Mechanical Brain Template* (c), which applies a continuum-mechanical transformation to each brain before intensity averaging. Scans are elastically reconfigured into a group mean configuration, using surface-based warping to match 84 surface models (including gyral pattern elements) across all subjects. Reconfigured scans are then averaged voxel-by-voxel, after intensity normalization, to produce a group image template with the average geometry *and* average image intensity for the group. Vector field transformations of extremely high spatial dimension (d),(e) are required to resolve cortical features, in their mean configuration, after scans are averaged together.

------

algorithm based on surface-driven elasticity [3,4,11]. These warping fields reconfigured each subject's 3D image into the average anatomic configuration for the group. By averaging the reconfigured images (after intensity normalization), a crisp image template was created to represent the group (Fig. 3(c)).

Note the better-resolved cortical features in the average images after high-dimensional cortical registration. If desired, this AD-specific atlas can retain the coordinate matrix of the Talairach system (with the anterior commissure at (0,0,0)) while refining the gyral map of the Talairach atlas to encode the unique anatomy of the AD population. By explicitly computing matching fields that relate gyral patterns across subjects, a well-resolved and spatially consistent set of probabilistic anatomical models and average images can be generated to represent the average anatomy and its variation in a subpopulation.

3 Results

3D Cortical Variability. 3D displacement fields were recovered mapping each patient into gyrus-by-gyrus correspondence with the average cortex (Fig. 3(e)), after affine differences between each individual brain and the average template were factored out. Anatomic variability was then defined at each point on the average cortical surface as the root mean square (r.m.s.) magnitude of the 3D displacement vectors, assigned to each point, in the surface maps driving individuals onto the group average [3,12-14]. A typical variability pattern (based on 20 subjects) is visualized as a color-coded map in Fig. 4(a),(b). Overall, variability values rose sharply (Fig. 4(a),(b)) from 4-5 mm in primary motor cortex to localized peaks of maximal variability in posterior perisylvian zones and superior frontal association cortex (16-18 mm). The regions of maximal variability, in temporo-parietal cortex, are areas of dramatic neuronal loss, early metabolic change, and perfusion deficits in mild to moderate AD. This suggests that extreme caution is necessary when referring to activation foci and metabolic deficits in this important area using stereotaxic coordinates, unless a non-linear registration approach is employed, otherwise structural differences may be interpreted as functional differences. The overall patterns of variation corroborate recent findings based on a fine-scale volumetric parcellation of the cortex [33], and suggest a greater morphologic individuality in cortical regions that are phylogenetically more recent.

Tensor Maps of Directional Variation. Structures do not vary to the same degree in every coordinate direction [12], and even these directional biases vary by cortical system. The principal directions of anatomic variability in a group can be shown in a *tensor map* (Figs. 4(a)-(c)). The maps have two uses. First, they make it easier to detect anomalies, which may be small in magnitude but in specific and unusual directions [3]. Second, they significantly increase the information content of Bayesian priors used for automated structure extraction and identification [34-37].

Population-Based Maps of Brain Asymmetry. Significant asymmetries in cortical organization become apparent in the average surface representations of anatomy for the group (Fig. 4(d)). The average Sylvian fissure terminates more posteriorly (by 10 mm; $p < 0.0002$) and is more horizontal on the left than on the right, corroborating
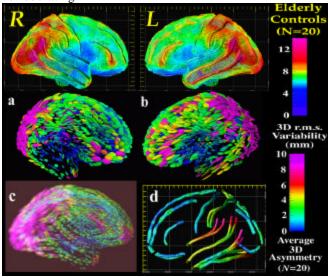

Figure 4. *Population-Based Maps of Cortical Variability and Asymmetry (N=20, Elderly Normals)*. Right (*R*) and left (*L*) hemisphere views show maps of 3D r.m.s. variability in cortical anatomy for 20 elderly normal subjects (all right handed, 10 males, 10 females). Residual variability in cortical patterning is shown after removing affine brain differences by linear transformation of the individual data to a group mean template (Fig. 3(c)). Ellipsoidal glyphs [(a)-(c)] indicate the principal directions of anatomical variation - they are most elongated along directions where anatomic variation is greatest across subjects. Each glyph represents the eigenvectors of the covariance tensor of the vector fields that map individual subjects onto their group average [3]. This covariance tensor determines the parameters of a multivariate Gaussian density for vector deviations at each point on the average cortical model [*transparent glyphs*, (c)]. Because gyral patterns constrain the mappings, the fields reflect variations in cortical organization at a more local level than can be achieved by only matching global cortical geometry. Note the elongated glyphs in anterior temporal cortex [(a)-(c)], and the very low variability (in any direction) in sensorimotor and inferior frontal areas. By better defining the parameters of allowable normal variations, the resulting information can be leveraged to distinguish normal from abnormal anatomical variants [3,32]. The magnitude of structural asymmetry in the brain is also clearly apparent (*asymmetry map*, N=20, (d)) in perisylvian cortex. The average right hemisphere cortical pattern is torqued forward (d) relative to the same cortical elements in the left brain hemisphere.
----

earlier *post mortem* findings. In a previous study, we found Sylvian fissure asymmetry to be significantly greater in AD ($p < 0.05$) than in control subjects matched for age, gender and handedness [14].

To determine whether these asymmetry patterns were also evident subcortically, average models of the underlying lateral ventricles (Fig. 4) were made for Alzheimer's patients and controls. As well as the prominent asymmetries of the occipital horn, disease-related differences in average ventricular anatomy were clearly localized (Fig. 5). By contrast with conventional volumetric approaches which show a *global* ventricular enlargement in AD, the region of greatest disease-related enlargement is clearly localized to the occipital horn. Anatomical averaging therefore reveals specific features of cortical and ventricular organization that are not observed in individual representations due to their considerable cross-subject variability.
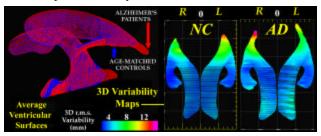

Fig. 5. *Population-Based Maps of Average Ventricular Anatomy in Normal Aging and Alzheimer's Disease*. In patients and controls, 3D parametric surface meshes [12] were used to model 14 ventricular elements, and meshes representing each surface element were averaged by hemisphere in each group. An average model for Alzheimer's patients (*red;* AD) is superimposed on an average model for matched normal controls (*blue;* NC). Mesh averaging reveals enlarged occipital horns in the Alzheimer's patients, and high stereotaxic variability in both groups. Extreme variability at the occipital horn tips also contrasts sharply with the stability of septal and temporal ventricular regions. A top view of these averaged surface meshes reveals localized asymmetry, variability, and displacement within and between groups. These subcortical asymmetries emerge only after averaging of anatomical maps in large groups of subjects.

----

4 Conclusion

Encoding patterns of anatomical variation in diseased populations presents significant challenges. By presenting an atlasing scheme that treats intensity and geometric variation separately, we described the creation of well-resolved image templates (Fig. 3(c)) and probabilistic models of anatomy (Figs. 4,5) that reflect the average morphology of a group. The continual refinement of

anatomic templates ultimately will enable deformation-based morphometry in large image databases [3,38], and shows promise in linking imaging findings with demographic, genetic, and therapeutic parameters [6]. Atlased data on anatomic variability can also act as Bayesian prior information to guide algorithms for automated image registration and labeling [34,37,38]. The resulting atlases are expandable, and may be stratified into subpopulations according to clinical, demographic or genetic criteria.

We also described approaches for creating and averaging brain models. These techniques produce statistical maps of group differences, abnormalities, and patterns of variation and asymmetry. These maps and models are key components of disease-specific brain atlases. Additional registration algorithms also transfer *post mortem* maps into the atlas, to correlate them with functional and metabolic data. The result is a multi-modality atlas that relates cognitive and functional measures with the cellular and pathologic hallmarks of the disease (Fig. 1; [9,10]).

As well as disease-specific atlases reflecting brain structure in dementia [5], research is underway to build a population-based brain atlas in schizophrenia based on large cohorts of medicated and first episode patients, as well as twins discordant for the disease [32]. Dynamic brain atlases are also being built to retain probabilistic information on growth rates in development and degeneration [6,7]. Refinement of these atlas systems to support dynamic and disease-specific data should generate an exciting framework to investigate variations in brain structure and function in large human populations.

6 References

[1]. Mazziotta JC, Toga AW, Evans AC, Fox P, Lancaster J (1995) A Probabilistic Atlas of the Human Brain: Theory and Rationale for its Development, NeuroImage 2: 89-101.

[2]. Grenander U, Miller MI (1998). Computational Anatomy: An Emerging Discipline, Technical Report, Dept. of Mathematics, Brown University.

[3]. Thompson PM, MacDonald D, Mega MS, Holmes CJ, Evans AC, Toga AW (1997). Detection and Mapping of Abnormal Brain

Structure with a Probabilistic Atlas of Cortical Surfaces, J. Comp. Assist. Tomogr. 21(4):567-581, Jul.-Aug. 1997.

[4]. Thompson PM, Toga AW (2000). *Elastic Image Registration and Pathology Detection*, Bankman I et al. [eds.], Handbook of Medical Image Processing, Academic Press, 2000.

[5]. Thompson PM, Mega MS, Toga AW (2000a). Disease-Specific Brain Atlases, in Mazziotta JC et al., [eds.], Brain Mapping: The Disorders, Academic Press.

[6]. Thompson PM, Narr KL, Blanton RE, Toga AW (2000b). *Mapping Structural Alterations of the Corpus Callosum during Brain Development and Degeneration*, in: Iacoboni M, Zaidel E [eds.], *The Corpus Callosum*, MIT Press [in press].

[7]. Thompson PM, Giedd JN, Woods RP, MacDonald D, Evans AC, Toga AW (2000c). *Growth Patterns in the Developing Human Brain Detected Using Continuum-Mechanical Tensor Mapping*, Nature 404:190-193, March 9, 2000.

[8]. Mega MS, Thompson PM, Toga AW, Cummings JL (2000). Brain Mapping in Dementia, in Mazziotta JC et al., [eds.], Brain Mapping: The Disorders, Academic Press.

[9]. Mega MS, Chen S, Thompson PM, Woods RP, Karaca TJ, Tiwari A, Vinters H, Small GW, Toga AW (1997) Mapping Pathology to Metabolism: Coregistration of Stained Whole Brain Sections to PET in Alzheimer's Disease, NeuroImage 5:147-153.

[10]. Mega MS, Chu T, Mazziotta JC, Trivedi KH, Thompson PM, Shah A, Cole G, Frautschy SA, Toga AW (1999). *Mapping Biochemistry to Metabolism: FDG-PET and Beta-Amyloid Burden in Alzheimer's Disease*, NeuroReport 10(14):2911-2917, Sept. 29 1999.

[11]. Thompson PM, Toga AW (1996a). A Surface-Based Technique for Warping 3-Dimensional Images of the Brain, IEEE Transactions on Medical Imaging, 15(4):1-16.

[12]. Thompson PM, Schwartz C, Lin RT, Khan AA, Toga AW (1996b). 3D Statistical Analysis of Sulcal Variability in the Human Brain, Journal of Neuroscience, Jul. 1996, 16(13):4261-4274.

[13]. Thompson PM, Schwartz C, Toga AW (1996c). High-Resolution Random Mesh Algorithms for Creating a Probabilistic 3D Surface Atlas of the Human Brain, NeuroImage 3:19-34.

[14]. Thompson PM, Moussai J, Khan AA, Zohoori S, Goldkorn A, Mega MS, Small GW, Cummings JL, Toga AW (1998). Cortical Variability and Asymmetry in Normal Aging and Alzheimer's Disease, Cerebral Cortex 8(6):492-509, Sept.1998.

[15]. Thompson PM, Toga AW (1997) Detection, Visualization and Animation of Abnormal Anatomic Structure with a Deformable Probabilistic Brain Atlas based on Random Vector Field Transformations, Medical Image Analysis 1(4):271-294.

[16]. Talairach J, Tournoux P (1988). Co-planar Stereotaxic Atlas of the Human Brain, New York: Thieme.

[17]. Zijdenbos AP, Dawant BM (1994). Brain Segmentation and White Matter Lesion Detection in MR Images, Crit. Rev. Biomed. Eng. 22(5-6):401-465.

[18]. MacDonald D (1998). A Method for Identifying Geometrically Simple Surfaces from Three Dimensional Images, PhD Thesis, McGill Univ., Canada.

[19]. Ono M, Kubik S, Abernathey CD (1990) Atlas of the Cerebral Sulci. Stuttgart: Thieme.

[20]. Ge Y, Fitzpatrick JM, Kessler RM, Jeske-Janicka M (1995). *Intersubject Brain Image Registration using both Cortical and Subcortical Landmarks*, SPIE Image Processing 2434:81-95.

[21]. Collins DL, Le Goualher G, Venugopal R, Caramanos A, Evans AC, Barillot C (1996). *Cortical Constraints for Non-Linear Cortical Registration*, In: Höhne KH, Kikinis R, [eds.], VBC'96, Hamburg, SPIE vol. 1131:307-316.

[22]. Davatzikos C (1996). *Spatial Normalization of 3D Brain Images using Deformable Models*, J. Comp. Assist. Tomogr. 20(4):656-665, Jul.-Aug. 1996.

[23]. Drury HA, Van Essen DC (1997) Analysis of Functional Specialization in Human Cerebral Cortex using the Visible Man Surface Based Atlas, Human Brain Mapping 5:233-237.

[24]. Fischl B, Sereno MI, Tootell RBH, Dale AM (1999). High-Resolution Inter-Subject Averaging and a Coordinate System for the Cortical Surface, [in press].

[25]. Einstein A (1914). *Covariance Properties of the Field Equations of the Theory of Gravitation Based on the Generalized Theory of Relativity,* Zeitschrift für Mathematik und Physik **63** (1914): 215-225.

[26]. Joshi SC, Miller MI, Christensen GE, Banerjee A, Coogan TA, Grenander U (1995). Hierarchical Brain Mapping via a Generalized Dirichlet Solution for Mapping Brain Manifolds, SPIE 2573:278-289.

[27]. Liseikin VD (1991). On a Variational Method for Generating Adaptive Grids on NDimensional Surfaces, Doklady Akademii Nauk. CCCP, 1991, V319 N3:546-549.

[28]. Evans AC, Collins DL, Neelin P, MacDonald D, Kamber M, Marrett TS (1994). Three-Dimensional Correlative Imaging: Applications in Human Brain Mapping, in: Functional Neuroimaging: Technical Foundations, Thatcher RW, Hallett M, Zeffiro T, John ER, Huerta M [eds.], 145-162.

[29]. Bookstein FL (1997). Landmark Methods for Forms Without Landmarks: Morphometrics of Group Differences in Outline Shape, Medical Image Analysis 1(3):225-243.

[30]. Woods RP, Mazziotta JC, Cherry SR (1993). MRI-PET Registration with Automated Algorithm, Journal of Computer Assisted Tomography 17:536-546.

[31]. Woods RP, Grafton ST, Watson JDG, Sicotte NL, Mazziotta JC (1993). *Automated image registration: II. Intersubject validation of linear and nonlinear models*. J. Computer Assisted Tomography 22.

[32]. Narr KL, Thompson PM, Sharma T, Moussai J, Cannestra AF, Toga AW (2000). *Mapping Corpus Callosum Morphology in Schizophrenia*, Cerebral Cortex 10(1):40-49, Jan. 2000.

[33]. Kennedy DN, Lange N, Makris N, Bates J, Meyer J, Caviness VS Jr. (1998). Gyri of the human neocortex: an MRI-based analysis of volume and variance. Cereb. Cortex 8(4):372-84.

[34]. Gee JC, LeBriquer L, Barillot C, Haynor DR, Bajcsy R (1995). Bayesian Approach to the Brain Image Matching Problem, Inst. for Res. in Cogn. Sci. Technical Report 95-08, April 1995.

[35]. Mangin J-F, Frouin V, Bloch I, Regis J, Lopez-Krahe J (1994). *Automatic Construction of an Attributed Relational Graph Representing the Cortex Topography using Homotopic Transformations*, SPIE 2299, 110-121.

[36]. Royackkers N, Desvignes M, Revenu M (1996). Construction automatique d'un atlas adaptatif des sillons corticaux, ORASIS 96, Clermont-Ferrand, pp. 187-192.

[37]. Pitiot A, Thompson PM, Toga AW (2000). *Spatially and Temporally Adaptive Elastic Template Matching*, IEEE Transactions on Pattern Analysis and Machine Intelligence, 2000.

[38]. Ashburner J, Hutton C, Frackowiak R, Johnsrude I, Price C, Friston K (1998). Identifying global anatomical differences: deformation-based morphometry. Hum Brain Mapp 6(5-6):348-57.

……………………………………